

# Entropy stable discontinuous Galerkin approximation for the Relativistic Hydrodynamic Equations

Biswarup Biswas\* and Harish Kumar†

Department of Mathematics,  
Indian Institute of Technology Delhi, New Delhi, India

## Abstract

This paper presents the higher-order discontinuous Galerkin entropy stable schemes for special relativistic hydrodynamic equations. A suitable entropy conservative flux is used to construct the scheme. It is studied that the presented fourth-order scheme provides less oscillatory approximation than the third-order scheme. Bound preserving limiter is used to keep the computed solution in the physical domain. Extensive numerical results are presented to validate the accuracy and robustness of the schemes.

**Keywords**— Discontinuous Galerkin scheme, entropy stability, high-order accurate scheme, special relativistic hydrodynamics

## 1 Introduction

Relativistic hydrodynamic equations can be used to model several astrophysical problems including  $\gamma$ -ray bursts, astrophysical jets, core-collapse supernovae, formation of black holes etc. We consider the equations of special relativistic hydrodynamics (RHD) with the ideal equation of state. Evolution of numerical scheme for RHD equations started with the work of Wilson [28, 29]. Riemann solvers for RHD equations are studied in several articles (see, [17, 18, 7, 13]). Development and advancement of the piece-wise parabolic reconstruction methods is done in [1, 19, 22]. A scheme using TVD reconstruction is implemented in [6]. High order ENO and WENO schemes are also applied to the RHD equations ([27, 9]). Meanwhile, there are several numerical schemes developed which can be found in the review article [10]. Recent works include the physical-constraint-preserving finite difference scheme for RHD equations by Wu and Tang [30]. More recently, the physical-constraint-preserving and bound preserving discontinuous Galerkin (DG) schemes are developed in [32, 24].

An unavoidable non-linear stability of numerical scheme for conservation laws is the entropy stability (see [26, 14, 4, 15, 25]). Entropy stable schemes are developed to find the unique physical solution of hyperbolic conservation laws as the weak solutions are not unique. Entropy stability of a scheme also additionally provides the  $L^2$  stability of the approximation (see [26]). A finite difference entropy stable scheme for RHD equations is developed very recently in [2].

In this article, we approximate the RHD system using entropy stable higher-order nodal DG scheme. We utilize the nodal DG spectral element method (DGSEM), which is used in [5] and [16] to approximate the Euler equations of gas-dynamics and ideal compressible MHD equations, respectively. The idea is to

---

\*biswarupb7@gmail.com

†hkumar@maths.iitd.ac.in

perform the integration in DG space using Gauss-Lobatto quadrature and then utilize the summation-by-parts (SBP) property of the difference matrix to write the well known weak and strong form of the DG scheme. Finally, to achieve the entropy stability, the scheme is reformulated by replacing point flux to entropy conservative flux and interface flux to some entropy stable Riemann solver.

## 2 RHD equations

The relativistic hydrodynamic model contains the following set of non-linear hyperbolic equations,

$$\frac{\partial D}{\partial t} + \nabla \cdot (D\mathbf{u}) = 0, \quad (1a)$$

$$\frac{\partial \mathbf{m}}{\partial t} + \nabla \cdot (\mathbf{m}\mathbf{u} + p\mathbf{I}) = 0, \quad (1b)$$

$$\frac{\partial E}{\partial t} + \nabla \cdot \mathbf{m} = 0. \quad (1c)$$

Here  $D$  is the mass,  $\mathbf{m}$  is the momentum vector,  $p$  is the pressure and  $E$  is the total energy. The fluid density  $\rho$ , velocity field  $u$ , and pressure  $p$  are related to the conservative quantities  $\mathbf{w} = [D, \mathbf{m}, E]^T$  as

$$D = \Gamma\rho, \quad \mathbf{m} = \rho h\Gamma^2\mathbf{u}, \quad E = \rho h\Gamma^2 - p,$$

where  $\Gamma$  and  $h$  are Lorentz factor and special enthalpy respectively.

In this work, we consider the two-dimensional RHD model which can be written in the conservative form,

$$\frac{\partial \mathbf{w}}{\partial t} + \frac{\partial \mathbf{f}_1}{\partial x} + \frac{\partial \mathbf{f}_2}{\partial y} = 0. \quad (2)$$

The fluxes are given by,

$$\mathbf{f}_1 = \begin{bmatrix} Du_x \\ m_x u_x + p \\ m_y u_x \\ m_x \end{bmatrix}, \text{ and } \mathbf{f}_2 = \begin{bmatrix} Du_y \\ m_x u_y \\ m_y u_y + p \\ m_y \end{bmatrix}.$$

Using the specific heat ratio  $\gamma$ , for the ideal equation of state the special enthalpy is given by

$$h = 1 + \frac{\gamma}{\gamma - 1} \frac{p}{\rho}.$$

### 2.1 Entropy function for RHD

We find weak solution of conservation laws which are not unique. A unique ‘physically relevant’ solution satisfies an entropy condition. To state the entropy condition, we recall some basic definitions and results.

**Definition 2.1.** A convex function  $\mathcal{U}$  is said to be an entropy function for conservation laws (2) if there exist smooth functions  $\mathcal{F}_j (j = 1, 2)$  such that

$$\mathcal{F}'_j = \mathcal{U}'(\mathbf{w})\mathbf{f}'_j(\mathbf{w}). \quad (3)$$

For RHD equations (2), the entropy functions and corresponding entropy flux functions are given by,

$$\mathcal{U} = -\frac{\rho\Gamma s}{\gamma - 1}, \quad \mathcal{F}_1 = -\frac{\rho\Gamma s u_x}{\gamma - 1}, \quad \mathcal{F}_2 = -\frac{\rho\Gamma s u_y}{\gamma - 1}, \quad (4)$$

where  $s = \ln(p\rho^{-\gamma})$  is the thermodynamic entropy. Smooth solutions of (2) satisfy the following additional conservation law (see [2]),

$$\frac{\partial \mathcal{U}}{\partial t} + \frac{\partial \mathcal{F}_1}{\partial x} + \frac{\partial \mathcal{F}_2}{\partial y} = 0. \quad (5)$$

For non-smooth solution the entropy condition is converted to the entropy inequality,

$$\frac{\partial \mathcal{U}}{\partial t} + \frac{\partial \mathcal{F}_1}{\partial x} + \frac{\partial \mathcal{F}_2}{\partial y} \leq 0. \quad (6)$$

### 3 Entropy stable high order DG schemes

We assume the spatial domain is compactly supported or periodic, and the time is continuous. We also concentrate on the one dimensional spacial domain. Extension of the scheme to the two-dimensional rectangular domain can be quickly done using the tensor product.

The spatial domain is partitioned into  $N$  elements  $I_i = [x_{i-\frac{1}{2}}, x_{i+\frac{1}{2}}]$  ( $1 \leq i \leq N$ ). Then in DG approach we find the solution,  $\mathbf{w}_h \in \mathbf{V}_h^k := \left\{ \mathbf{v}_h : \mathbf{v}_h|_I \in [\mathcal{P}^k(I)]^4, 1 \leq i \leq N \right\}$  such that for all  $\mathbf{v}_h \in \mathbf{V}_h^k$  and for all  $1 \leq i \leq N$ ,

$$\begin{aligned} \int_I \frac{\partial \mathbf{w}_h^T}{\partial t} \mathbf{v}_h dx - \int_I \mathbf{f}_1(\mathbf{w}_h)^T \frac{d\mathbf{v}_h}{dx} dx \\ + \hat{\mathbf{f}}_{1,i+1/2}^T \mathbf{v}_h(x_{i+1/2}^-) - \hat{\mathbf{f}}_{1,i-1/2}^T \mathbf{v}_h(x_{i-1/2}^+) = 0, \end{aligned} \quad (7)$$

where  $\hat{\mathbf{f}}_{1,i+1/2}$  is an numerical flux depends on the numerical solutions at element interface, that is,  $\hat{\mathbf{f}}_{1,i+1/2} = \hat{\mathbf{f}}_1(\mathbf{w}_h(x_{i+1/2}^-), \mathbf{w}_h(x_{i+1/2}^+))$ .

#### 3.1 Gauss-Lobatto quadrature and summation-by-parts

Use of Gauss-Lobatto quadrature for the integrals is one of the key ideas in [11, 5] to define the entropy stable DG schemes. Consider a reference element  $I = [-1, 1]$ . Then  $k$  Gauss-Lobatto quadrature points are taken as,

$$-1 = \xi_0 < \xi_1 < \xi_2 \dots < \xi_k = 1$$

with corresponding quadrature weights  $\omega_j$ ,  $0 \leq j \leq k$ . Define

$$\langle u, v \rangle := \int_I u v d\xi, \quad (8)$$

$$\langle u, v \rangle_h := \sum_{j=0}^k \omega_j u(\xi_j) v(\xi_j). \quad (9)$$

Then using the Lagrange(nodal) basis,

$$L_j(\xi) = \prod_{l=0, l \neq j}^N \frac{\xi - \xi_l}{\xi_j - \xi_l},$$

we define matrices  $D$ ,  $M$ , and  $S$  as follows,

$$\begin{cases} D_{jl} = L_l'(\xi_j), \\ M_{jl} = \langle L_j, L_l \rangle_h = \omega_j \delta_{jl}, \\ S_{jl} = \langle L_j, L_l' \rangle_h = \langle L_j, L_l' \rangle. \end{cases}$$

**Theorem 3.1** (SBP property ([3])). *The following discrete analogue of integration by parts, known as summation-by-parts (SBP) holds:*

$$\begin{cases} S = MD, \\ MD + D^T M = S + S^T = B. \end{cases}$$

where the  $B$  is known as the boundary matrix given by,

$$B = \text{diag}\{\tau_0, \tau_1, \dots, \tau_k\}, \quad \tau_j := \begin{cases} -1 & j = 0 \\ 0 & 1 \leq j \leq k-1 \\ 1 & j = k \end{cases}.$$

Then on using SBP operators and applying Gauss-Lobatto quadrature in (7) one can write the following DG scheme for a single element [5]:

$$\frac{\Delta x}{2} \frac{d\mathbf{w}^p}{dt} + \sum_{l=0}^k 2D_{pl} \mathbf{f}_1^*(\mathbf{w}^p, \mathbf{w}^l) = \frac{\tau_p}{\omega_p} (\mathbf{f}_1^p - \hat{\mathbf{f}}_1^p), \quad p = 0, 1, \dots, k \quad (10)$$

where the following notations are used, and index  $i$  is dropped,

$$x_i(\xi) = \frac{1}{2}(x_{i-1/2} + x_{i+1/2}) + \frac{\xi}{2}\Delta x_i,$$

$$\mathbf{w}^l = \mathbf{w}_h(x_i(\xi_l)), \quad \mathbf{f}_1^l = \mathbf{f}_1(\mathbf{w}^l), \quad l = 0, 1, \dots, k$$

$$[\hat{\mathbf{f}}_1^0, \hat{\mathbf{f}}_1^1, \dots, \hat{\mathbf{f}}_1^k] = [\hat{\mathbf{f}}_{1i-1/2}, 0, \dots, 0, \hat{\mathbf{f}}_{1i+1/2}].$$

Here  $\mathbf{f}_1^*$  is a two-point entropy conservative flux defined in [2]. We recall the definition of entropy conservative flux.

**Definition 3.1.** A two point symmetric, consistent numerical flux is said to be entropy conservative flux for an entropy function  $\mathcal{U}$  if

$$(\mathbf{v}_R - \mathbf{v}_L)^T \mathbf{f}^*(\mathbf{w}_R, \mathbf{w}_L) = \psi_R - \psi_L, \quad (11)$$

where  $\mathbf{v} = \mathcal{U}'(\mathbf{w})$  is known as entropy variable, and  $\psi = \mathbf{v}^T \cdot \mathbf{f} - \mathcal{F}$  is the entropy potential.  $L$  and  $R$  in suffix denote the left and right state.

**Definition 3.2.** A two-point symmetric, consistent numerical flux is said to be entropy stable flux for the entropy function  $\mathcal{U}$  if

$$(\mathbf{v}_R - \mathbf{v}_L)^T \mathbf{f}^*(\mathbf{w}_R, \mathbf{w}_L) \leq \psi_R - \psi_L. \quad (12)$$

**Theorem 3.2** ([5]). If  $\mathbf{f}_1^*(\mathbf{w}_L, \mathbf{w}_R)$  is consistent and symmetric, then (10) is conservative and high order accurate. If we further assume that  $\mathbf{f}_1^*(\mathbf{w}_L, \mathbf{w}_R)$  is entropy conservative, then (10) is also locally entropy conservative within a single element.

For proof one can look into [5]

For RHD equations we use the entropy conservative flux proposed in [2] which is given by,

$$\begin{aligned} \mathbf{f}_1^{*(1)} &= \hat{\rho} \bar{\mu}_x \\ \mathbf{f}_1^{*(2)} &= \frac{\bar{\mu}_x}{\bar{\Gamma}} \mathbf{f}_1^{*(4)} + \frac{\bar{\rho}}{\beta} \\ \mathbf{f}_1^{*(3)} &= \frac{\bar{\mu}_y}{\bar{\Gamma}} \mathbf{f}_1^{*(4)} \\ \mathbf{f}_1^{*(4)} &= - \frac{\bar{\Gamma} \left( k_1 \hat{\rho} \bar{\mu}_x + \frac{\bar{\mu}_x \bar{\rho}}{\beta} \right)}{\bar{\mu}_x^2 + \bar{\mu}_y^2 - \bar{\Gamma}^2} \end{aligned}$$

where  $k_1 = 1 + \frac{1}{\gamma - 1} \frac{1}{\beta}$ ,  $\mu_x = \Gamma u_x$ ,  $\mu_y = \Gamma u_y$  and  $\hat{a} := \frac{a_R - a_L}{\ln a_R - \ln a_L}$ .

**Theorem 3.3.** *If the numerical flux  $\hat{\mathbf{f}}_1$  at the element interface is entropy stable, then the scheme (10) is entropy stable.*

The entropy production rate at the interface is

$$\begin{aligned} & (\psi_k^i - (\mathbf{v}_k^i)^T \hat{\mathbf{f}}_1(\mathbf{w}_k^i, \mathbf{w}_0^{i+1})) - (\psi_0^{i+1} - (\mathbf{v}_0^{i+1})^T \hat{\mathbf{f}}_1(\mathbf{w}_k^i, \mathbf{w}_0^{i+1})) \\ &= (\mathbf{v}_0^{i+1} - \mathbf{v}_k^i)^T \hat{\mathbf{f}}_1(\mathbf{w}_k^i, \mathbf{w}_0^{i+1}) - (\psi_0^{i+1} - \psi_k^i). \end{aligned}$$

The expression clearly shows that the scheme (10) is entropy stable if the numerical flux  $\hat{\mathbf{f}}_1$  at the element interface is entropy stable.

**Note 1.** *TVD/TVB limiters and bounds preserving limiters can be used for enhancing the performance for the scheme. We have utilized the bounds preserving limiter given in [24] to keep the solution in physical space. We recall from [5] that the use of bounds preserving limiter will not increase the entropy.*

## 4 Numerical results

The semi-discrete scheme (10) is integrated using the standard third order strong stability preserving (SSP) Runge-Kutta method [12]. The computational domain is set to be  $[0, 1]$  for the one-dimensional problems, and  $[0, 1] \times [0, 1]$  for the two-dimensional problems unless stated separately. We also set  $\gamma = \frac{5}{3}$ . The  $\mathbf{p}$ -th order scheme is termed as ESDG-Op.

### One dimensional(1D) problems

We have used 200 grids for all the 1D problems. Lax-Friedrich flux is used as the element interface flux. We have also used a fixed  $CFL = 0.1$  for all computations. For the Riemann problems we plot the results along with the exact Riemann solver given in [20]

**Test Problem 1. Accuracy test** To check the accuracy of the scheme, we consider the following smooth initial conditions with periodic boundary,

$$(\rho, u, p) = (2 + \sin(2\pi x), 0.5, 1).$$

We compute up-to a final time  $t = 2$  and error is calculated using the exact solution  $\rho(x, 2) = 2 + \sin(2\pi(x - 2))$ . Table 1 and Table 2 show that the schemes achieved their desired order of accuracy.

N	$L^1$ error	Order	$L^\infty$ error	Order
32	4.18e-04	...	4.33e-04	...
64	5.41e-05	2.95	5.52e-05	2.97
128	6.86e-06	2.98	6.91e-06	3.00
256	8.63e-07	2.99	8.65e-07	3.00

Table 1: Accuracy table for ESDG-O3 scheme

**Test Problem 2. Isentropic Smooth Flows** We consider this smooth test from [31]. The problem consist of a pulse of width  $L = 0.3$  and amplitude  $\alpha = 1$  inside the domain  $[-0.35, 1]$ . We take a reference state  $(\rho_{ref}, u_{ref}, p_{ref}) = (1, 0, 100)$  outside the pulse. The initial density profile is given by

$$\rho = \rho_{ref} (1 + \alpha f(x)),$$

N	$L^1$ error	Order	$L^\infty$ error	Order
32	3.60e-06	...	6.63e-06	...
64	2.20e-07	4.03	4.07e-07	4.03
128	1.37e-08	4.01	2.53e-08	4.01
256	8.56e-10	4.00	1.58e-09	4.00

Table 2: Accuracy table for ESDG-O4 scheme

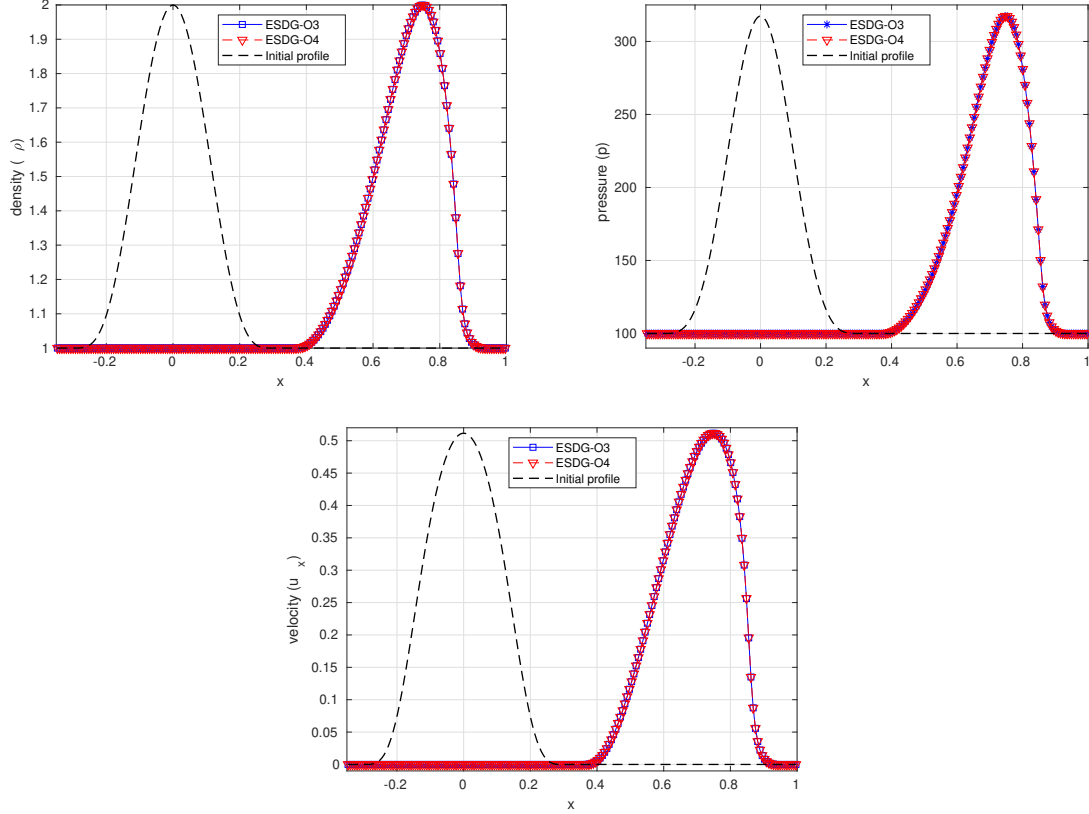


Figure 1: Solution at  $t = 0.8$  using  $CFL = 0.1$  on 200 grids

where

$$f(x) = \begin{cases} \left( \left( \frac{x}{L} \right)^2 - 1 \right)^4 & \text{if } |x| < L \\ 0 & \text{otherwise.} \end{cases}$$

Initial pressure is taken as  $p = K\rho^\gamma$ , where  $K$  is constant. The velocity inside the pulse is set such that the Riemann invariant,

$$J = \frac{1}{2} \ln \left( \frac{1+u}{1-u} \right) - \frac{1}{\sqrt{\gamma-1}} \ln \left( \frac{\sqrt{\gamma-1}+c}{\sqrt{\gamma-1}-c} \right)$$

remains constant throughout the region, where  $c$  is the sound speed. Figure 1 presents the computational results of ESDG-O3 and ESDG-O4 at time  $t = 0.8$ . Both the schemes maintain the initial height of the pulse very accurately.

**Test Problem 3.** Next we consider the following Riemann problem from [21].

$$(\rho, u, p) = \begin{cases} (1, -0.6, 10) & \text{if } x < 0.5 \\ (10, 0.5, 20) & \text{if } x > 0.5 \end{cases}.$$

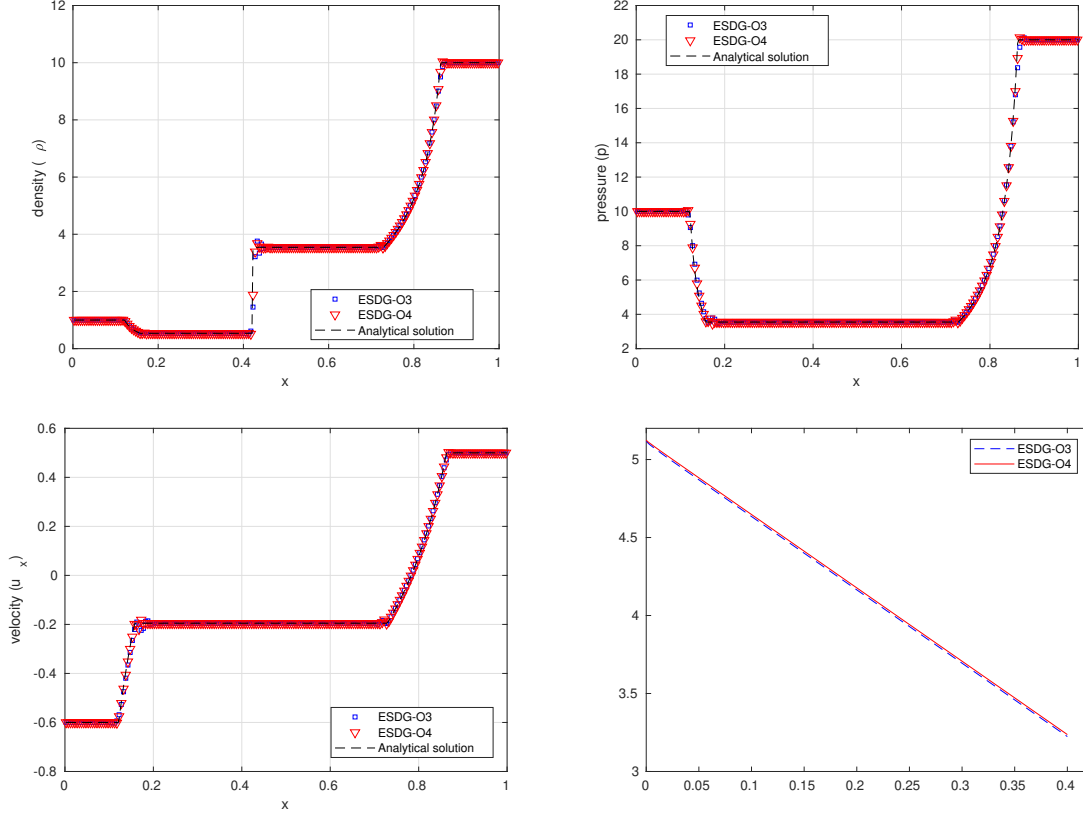


Figure 2: Solution at  $t = 0.4$  using  $CFL = 0.1$  on 200 grids

The solution contains two oppositely moving rarefaction separated by a contact wave. The computed solutions are presented in Figure 2 which shows that the schemes are able to capture the discontinuities well and entropy is gradually decreasing following the theoretical claims. It is also notable that the ESDG-O4 gives better results than ESDG-O3.

**Test Problem 4.** The Riemann problem (13) from [20] shows the wave capturing ability of a scheme.

$$(\rho, u, p) = \begin{cases} (1, 0, 10^3) & \text{if } x < 0.5 \\ (1, 0, 10^{-2}) & \text{if } x > 0.5 \end{cases} \quad (13)$$

Figure 3 shows that both the scheme captures the waves and ESDG-O4 gives notably better results than ESDG-O3.

**Test Problem 5.** We consider the following Riemann problem from [8].

$$(\rho, u, p) = \begin{cases} (5, 0, 50) & \text{if } x < 0.5 \\ (2 + 0.3 \sin(50x), 0, 5) & \text{if } x > 0.5 \end{cases}$$

The solution contains fluctuating smooth density waves which are challenging to capture by a scheme. Figure 4 shows that both the scheme ESDG-O3 and ESDG-O4 captures the smooth waves well.

## Two dimensional(2D) problems

For two dimensional problem, we extend the scheme (10) using the tensor product (see Appendix A). In this section, we will present the numerical results of the ESDG-O3 and ESDG-O4 schemes using  $CFL = 0.1$

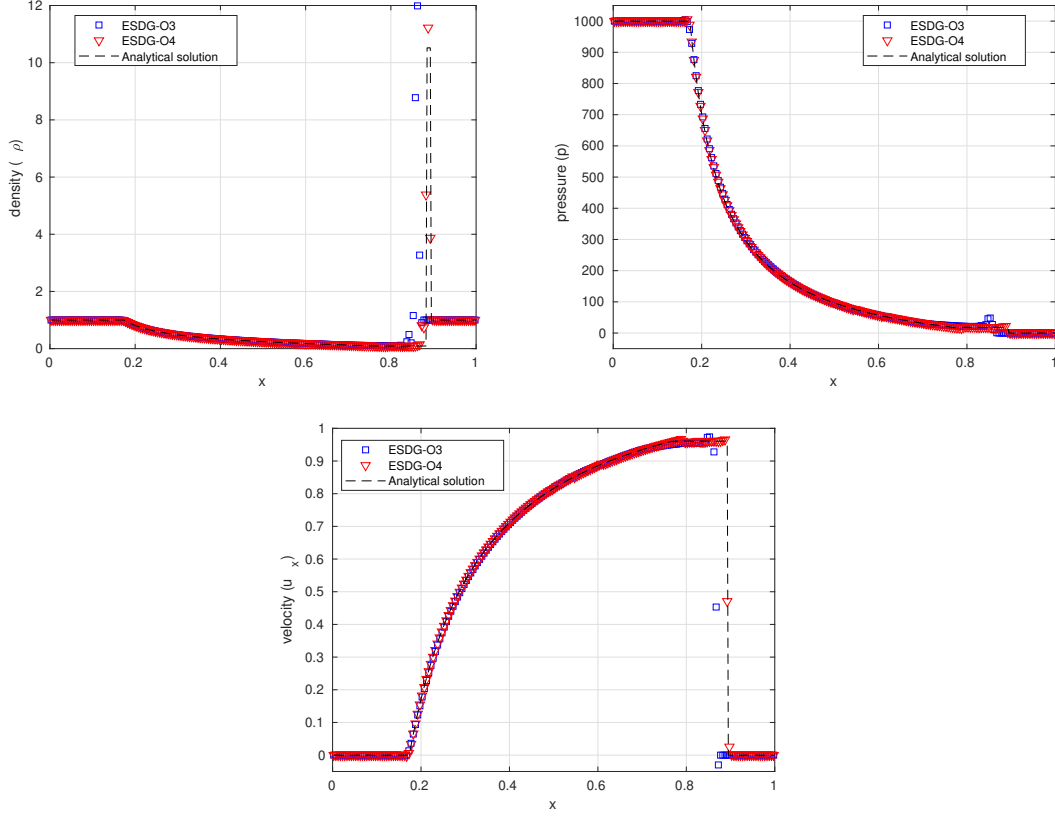


Figure 3: Solution at  $t = 0.4$  using  $CFL = 0.1$  on 200 grids

on a  $100 \times 100$  rectangular mesh. Bound preserving limiter is used together with local Lax-Friedrich flux as interface flux. We compute the solution until  $t = 0.4$  in all the two-dimensional test problems.

**Test Problem 6.** We present the following two-dimensional problem from [23].

$$(\rho, u_x, u_y, p) = \begin{cases} (0.5, 0.5, -0.5, 5) & \text{if } x > 0.5 \text{ and } y > 0.5 \\ (1, 0.5, 0.5, 5) & \text{if } x < 0.5 \text{ and } y > 0.5 \\ (3, -0.5, 0.5, 5) & \text{if } x < 0.5 \text{ and } y < 0.5 \\ (1.5, -0.5, -0.5, 5) & \text{if } x > 0.5 \text{ and } y < 0.5 \end{cases}$$

There is a four vortex sheets interaction in the center of the domain. The density solution contains a spiral with a very low value in the center. Computational results are plotted in Figure 5 which shows that both the scheme captures the flow geometry well. ESDG-O4 provides better resolution than the ESDG-O3 scheme.

**Test Problem 7.** Next we consider the initial conditions given by [23]

$$(\rho, u_x, u_y, p) = \begin{cases} (1, 0, 0, 1) & \text{if } x > 0.5 \text{ and } y > 0.5 \\ (0.5771, -0.3529, 0, 0.4) & \text{if } x < 0.5 \text{ and } y > 0.5 \\ (1, -0.3529, -0.3529, 1) & \text{if } x < 0.5 \text{ and } y < 0.5 \\ (0.5771, 0, -0.3529, 0.4) & \text{if } x > 0.5 \text{ and } y < 0.5 \end{cases}$$

In this problem rarefaction waves interacts and generates two symmetric shock waves. The results plotted in Figure 6 which shows that the schemes capture the rarefactions and shock waves with high resolution.



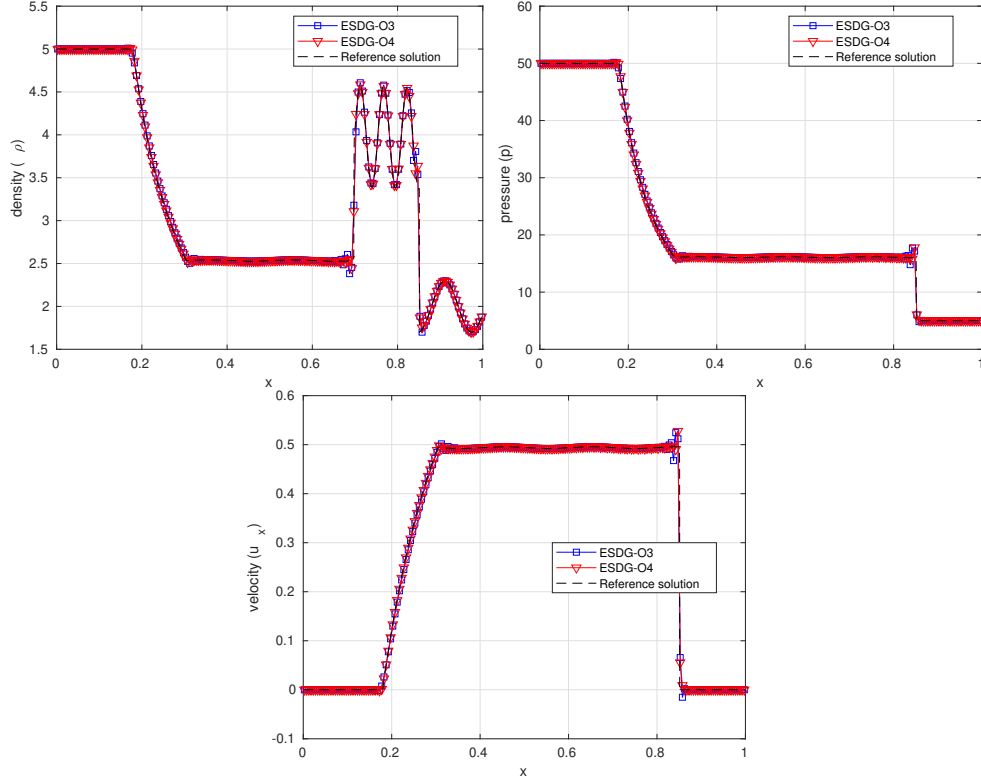


Figure 4: Solution at  $t = 0.4$  using  $CFL = 0.1$  on 200 grids

**Test Problem 8.** In this test case we consider the Riemann problem from [23] with initial primitives,

$$(\rho, u_x, u_y, p) = \begin{cases} (0.035145216124503, 0, 0, 0.162931056509027) & \text{if } x > 0.5 \text{ and } y > 0.5 \\ (0.1, 0.7, 0, 1) & \text{if } x < 0.5 \text{ and } y > 0.5 \\ (0.5, 0, 0, 1) & \text{if } x < 0.5 \text{ and } y < 0.5 \\ (0.1, 0, 0.7, 1) & \text{if } x > 0.5 \text{ and } y < 0.5 \end{cases}$$

The density solution contains two contact discontinuities on the south-west quadrant of the domain, and two curved front shocks in the north-east quadrant. Figure 7 shows that all the geometries are well captured by the schemes.

**Test Problem 9.** We consider the following Riemann problem with the high fluid velocity,

$$(\rho, u_x, u_y, p) = \begin{cases} (0.1, 0, 0, 20) & \text{if } x > 0.5 \text{ and } y > 0.5 \\ (0.00414329639576, 0.9, 0, 0.05) & \text{if } x < 0.5 \text{ and } y > 0.5 \\ (0.01, 0, 0, 0.05) & \text{if } x < 0.5 \text{ and } y < 0.5 \\ (0.00414329639576, 0, 0.9, 0.05) & \text{if } x > 0.5 \text{ and } y < 0.5 \end{cases}$$

The original problem presented in [30]. Numerical solution presented in Figure 8 shows that the ESDG-O3 and ESDG-O4 scheme give high resolution solution.

## 5 Conclusion

Higher-order entropy stable nodal DG solvers are used to solve RHD equations. It is noted that the presented ESDG-O4 scheme gives better results than the ESDG-O3 scheme. We have also observed that

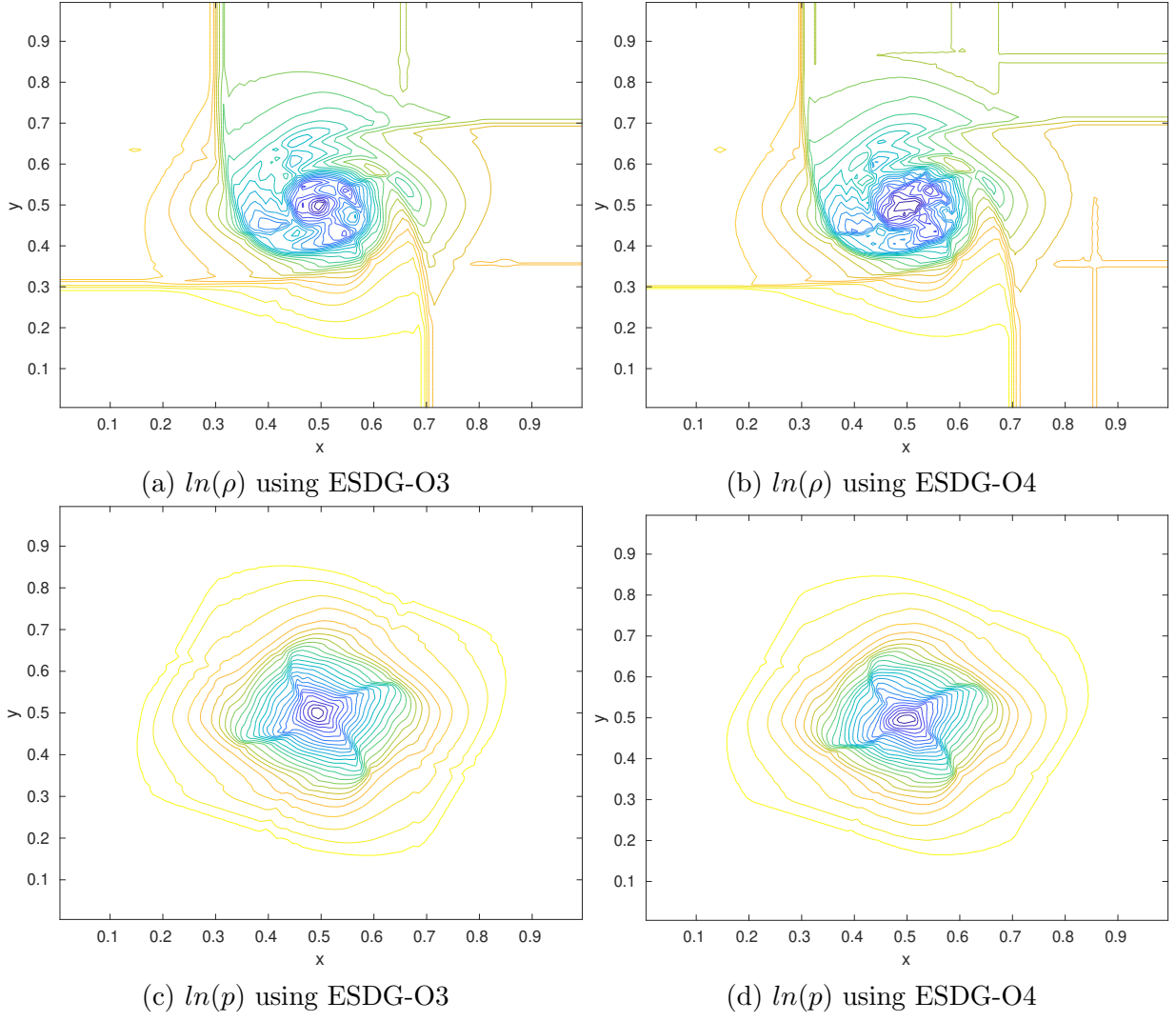


Figure 5: Plot of density and pressure in logarithmic scale using 25 contours at time  $t = 0.4$  using  $100 \times 100$  mesh.

the use of bound preserving limiter is necessary for some test cases to keep the solution in physical space. The presented schemes provide high-resolution solutions; however, mild oscillations are observed in some test cases.

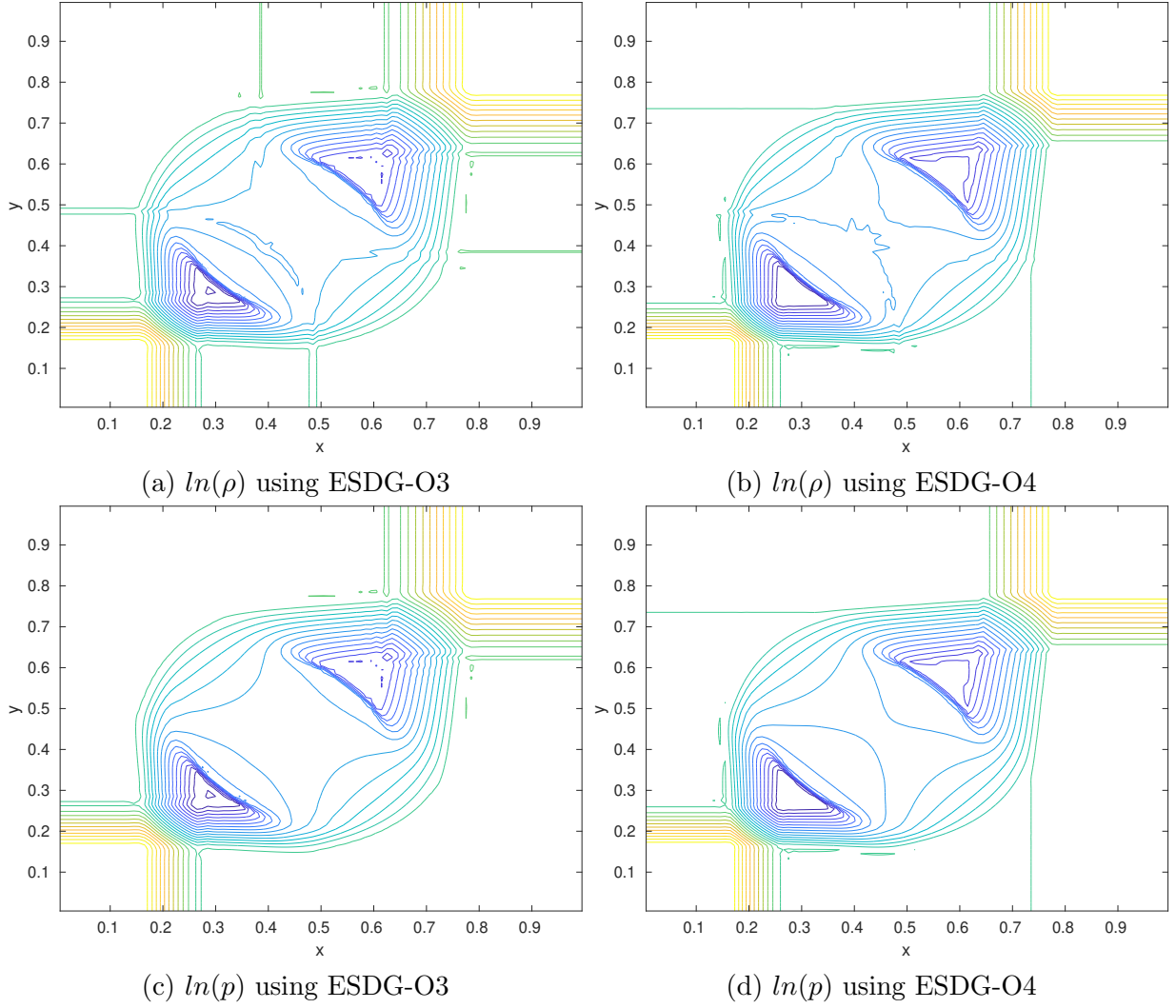


Figure 6: Plot of density and pressure in logarithmic scale using 25 contours at time  $t = 0.4$  using  $100 \times 100$  mesh.

## References

- [1] ALOY, M. A., IBÁÑEZ, J. M., MARTÍ, J. M., AND MÜLLER, E. Genesis: A high-resolution code for three-dimensional relativistic hydrodynamics. *The Astrophysical Journal Supplement Series* 122, 1 (1999), 151.
- [2] BHORIYA, D., AND KUMAR, H. Entropy Stable Schemes For Relativistic Hydrodynamics Equations. preprint, 2019.
- [3] CARPENTER, M. H., FISHER, T. C., NIELSEN, E. J., AND FRANKEL, S. H. Entropy Stable Spectral Collocation Schemes for the Navier–Stokes Equations: Discontinuous Interfaces. *SIAM Journal on Scientific Computing* 36, 5 (2014), B835–B867.
- [4] CHANDRASHEKAR, P. Kinetic energy preserving and entropy stable finite volume schemes for compressible euler and navier-stokes equations. *Communications in Computational Physics* 14, 5 (2013), 1252–1286.

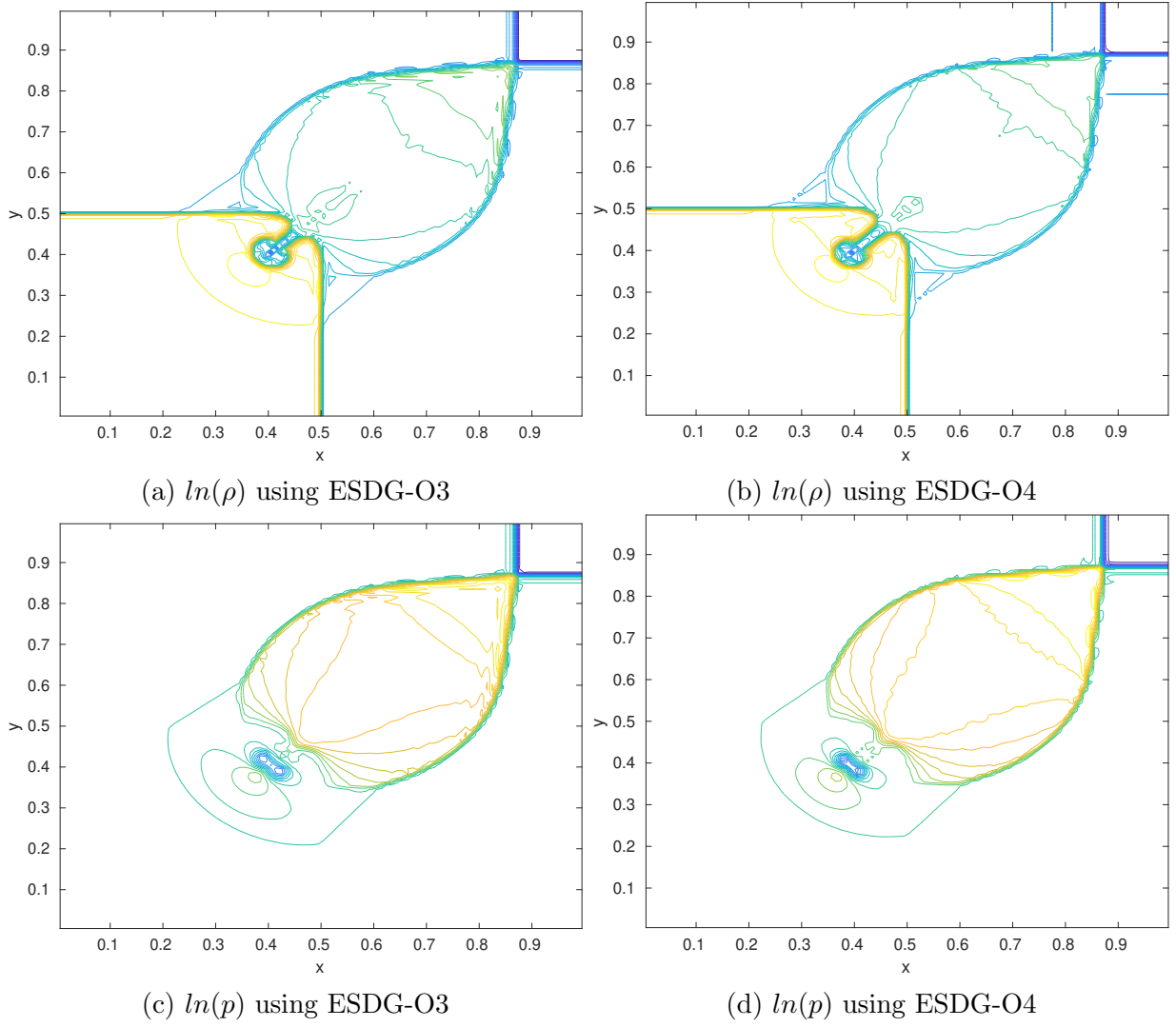


Figure 7: Plot of density and pressure in logarithmic scale using 25 contours at time  $t = 0.4$  using  $100 \times 100$  mesh.

- [5] CHEN, T., AND SHU, C.-W. Entropy stable high order discontinuous Galerkin methods with suitable quadrature rules for hyperbolic conservation laws. *Journal of Computational Physics* 345 (2017), 427–461.
- [6] CHOI, E., AND RYU, D. Numerical relativistic hydrodynamics based on the total variation diminishing scheme. *New Astronomy* 11, 2 (2005), 116–129.
- [7] DAI, W., AND WOODWARD, P. R. An iterative riemann solver for relativistic hydrodynamics. *SIAM Journal on Scientific Computing* 18, 4 (1997), 982–995.
- [8] DEL ZANNA, L., AND BUCCIANTINI, N. An efficient shock-capturing central-type scheme for multi-dimensional relativistic flows-i. hydrodynamics. *Astronomy & Astrophysics* 390, 3 (2002), 1177–1186.
- [9] DOLEZAL, A., AND WONG, S. Relativistic hydrodynamics and essentially non-oscillatory shock capturing schemes. *Journal of Computational Physics* 120, 2 (1995), 266–277.
- [10] FONT, J. A. Numerical hydrodynamics and magnetohydrodynamics in general relativity. *Living reviews in relativity* 11, 1 (2008), 7.

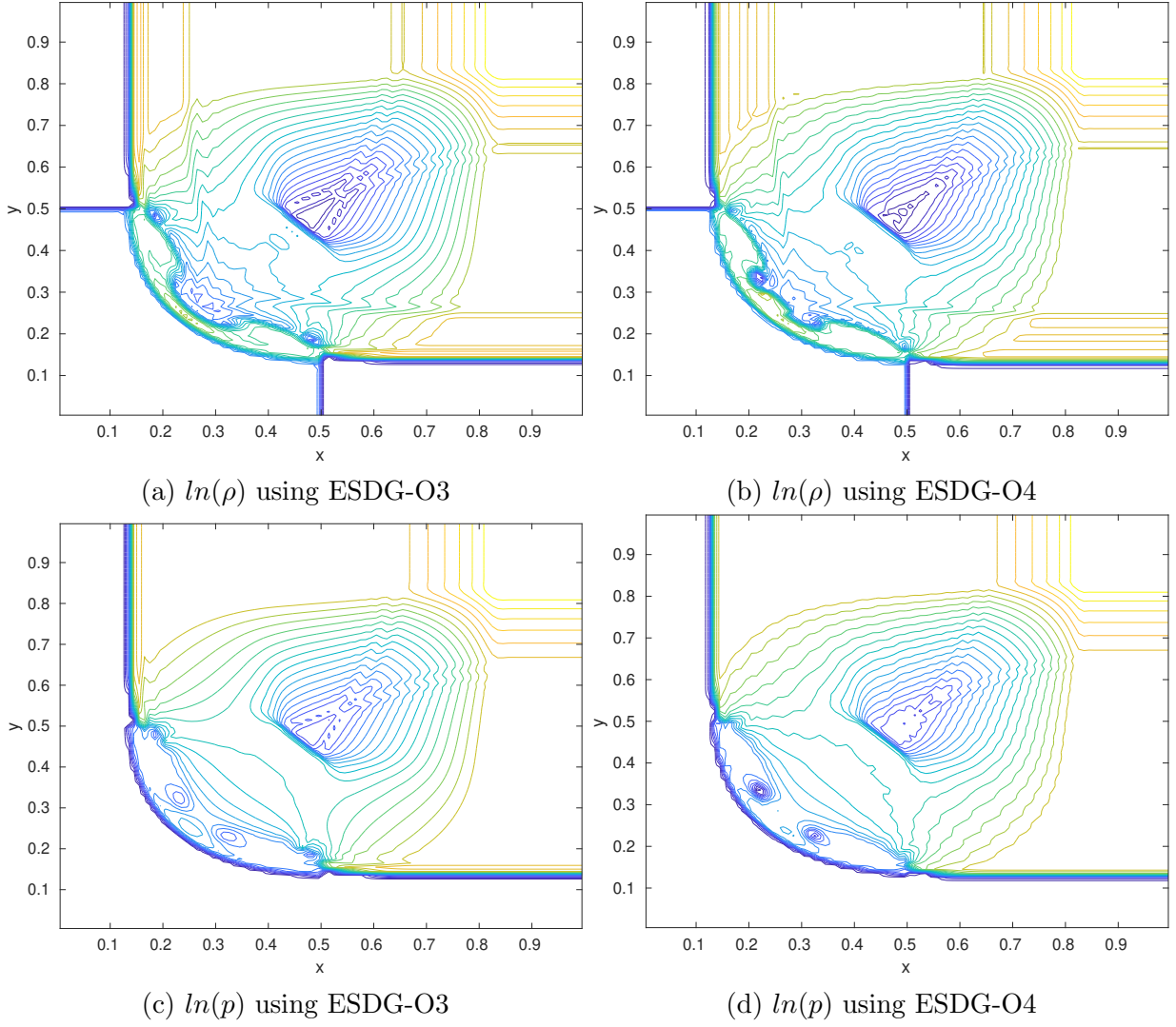


Figure 8: Plot of density and pressure in logarithmic scale using 25 contours at time  $t = 0.4$  using  $100 \times 100$  mesh.

- [11] GASSNER, G. J., WINTERS, A. R., AND KOPRIVA, D. A. A well balanced and entropy conservative discontinuous Galerkin spectral element method for the shallow water equations. *Applied Mathematics and Computation* 272 (2016), 291–308.
- [12] GOTTLIEB, S., SHU, C.-W., AND TADMOR, E. Strong stability-preserving high-order time discretization methods. *SIAM review* 43, 1 (2001), 89–112.
- [13] IBÁÑEZ, J. M., AND MARTÍ, J. M. Riemann solvers in relativistic astrophysics. *Journal of computational and applied mathematics* 109, 1-2 (1999), 173–211.
- [14] ISMAIL, F., AND ROE, P. L. Affordable, entropy-consistent euler flux functions ii: Entropy production at shocks. *Journal of Computational Physics* 228, 15 (2009), 5410–5436.
- [15] KUMAR, H., AND MISHRA, S. Entropy stable numerical schemes for two-fluid plasma equations. *Journal of scientific computing* 52, 2 (2012), 401–425.
- [16] LIU, Y., SHU, C.-W., AND ZHANG, M. Entropy stable high order discontinuous galerkin methods for ideal compressible mhd on structured meshes. *Journal of Computational Physics* 354 (2018), 163–178.

- [17] MARTÍ, J. M., IBÁÑEZ, J. M., AND MIRALLES, J. A. Numerical relativistic hydrodynamics: Local characteristic approach. *Phys. Rev. D* 43 (Jun 1991), 3794–3801.
- [18] MARTÍ, J. M., AND MÜLLER, E. The analytical solution of the riemann problem in relativistic hydrodynamics. *Journal of Fluid Mechanics* 258 (1994), 317333.
- [19] MARTÍ, J. M., AND MÜLLER, E. Extension of the piecewise parabolic method to one-dimensional relativistic hydrodynamics. *Journal of Computational Physics* 123, 1 (1996), 1–14.
- [20] MARTÍ, J. M., AND MÜLLER, E. Numerical Hydrodynamics in Special Relativity. *Living Reviews in Relativity* 6, 1 (dec 2003), 7.
- [21] MIGNONE, A., AND BODO, G. An HLLC Riemann solver for relativistic flows I. Hydrodynamics. *Monthly Notices of the Royal Astronomical Society* 364, 1 (11 2005), 126–136.
- [22] MIGNONE, A., PLEWA, T., AND BODO, G. The piecewise parabolic method for multidimensional relativistic fluid dynamics. *The Astrophysical Journal Supplement Series* 160, 1 (2005), 199.
- [23] NÚÑEZ-DE LA ROSA, J., AND MUNZ, C.-D. XTROEM-FV: a new code for computational astrophysics based on very high order finite-volume methods–II. Relativistic hydro-and magnetohydrodynamics. *Monthly Notices of the Royal Astronomical Society* 460, 1 (2016), 535–559.
- [24] QIN, T., SHU, C.-W., AND YANG, Y. Bound-preserving discontinuous galerkin methods for relativistic hydrodynamics. *Journal of Computational Physics* 315 (2016), 323 – 347.
- [25] SEN, C., AND KUMAR, H. Entropy stable schemes for ten-moment gaussian closure equations. *Journal of Scientific Computing* 75, 2 (2018), 1128–1155.
- [26] TADMOR, E. Entropy stability theory for difference approximations of nonlinear conservation laws and related time-dependent problems. *Acta Numerica* 12 (2003), 451–512.
- [27] TCHEKHOVSKOY, A., MCKINNEY, J. C., AND NARAYAN, R. wham: a WENO-based general relativistic numerical scheme I. Hydrodynamics. *Monthly Notices of the Royal Astronomical Society* 379, 2 (07 2007), 469–497.
- [28] WILSON, J. R. Numerical study of fluid flow in a kerr space. *The Astrophysical Journal* 173 (1972), 431.
- [29] WILSON, J. R. A numerical method for relativistic hydrodynamics. *Sources of Gravitational Radiation* (1979), 423–445.
- [30] WU, K., AND TANG, H. High-order accurate physical-constraints-preserving finite difference weno schemes for special relativistic hydrodynamics. *Journal of Computational Physics* 298 (2015), 539–564.
- [31] ZHANG, W., AND MACFADYEN, A. I. RAM: a relativistic adaptive mesh refinement hydrodynamics code. *The Astrophysical Journal Supplement Series* 164, 1 (2006), 255.
- [32] ZHAO, J., AND TANG, H. Runge-kutta central discontinuous galerkin methods for the special relativistic hydrodynamics. *Communications in Computational Physics* 22, 3 (2017), 643682.

## Appendix A Two dimensional scheme

We use the rectangular mesh  $I_{i,j} = \left[ x_{i-\frac{1}{2}}, x_{i+\frac{1}{2}} \right] \times \left[ y_{j-\frac{1}{2}}, y_{j+\frac{1}{2}} \right]$  ( $1 \leq i \leq N_x$ ), ( $1 \leq j \leq N_y$ ) with mesh size  $\Delta x_i$  and  $\Delta y_j$  in  $x$  and  $y$  direction respectively. For simplicity we consider the same number of Gauss-Lobatto points ( $k+1$ ) in both direction. Then for a single element  $I_{i,j}$ , the scheme is given by,

$$\begin{aligned} \frac{d\mathbf{w}^{p,q}}{dt} = & -\frac{2}{\Delta x} \left( \sum_{l=0}^k 2D_{pl} \mathbf{f}_1^*(\mathbf{w}^p, \mathbf{w}^l) - \frac{\tau_p}{\omega_p} (\mathbf{f}_1^{p,q} - \hat{\mathbf{f}}_1^{p,q}) \right) \\ & - \frac{2}{\Delta y} \left( \sum_{l=0}^k 2D_{ql} \mathbf{f}_2^*(\mathbf{w}^q, \mathbf{w}^l) - \frac{\tau_q}{\omega_q} (\mathbf{f}_2^{p,q} - \hat{\mathbf{f}}_2^{p,q}) \right), \quad (p, q = 0, 1, \dots, k) \end{aligned} \quad (14)$$

where we have used the following notations by dropping the indices  $i$  and  $j$ ,

$$\begin{aligned} x_i(\xi) &= \frac{1}{2}(x_{i-1/2} + x_{i+1/2}) + \frac{\xi}{2}\Delta x_i, \\ y_j(\xi) &= \frac{1}{2}(y_{j-1/2} + y_{j+1/2}) + \frac{\xi}{2}\Delta y_j, \\ \mathbf{w}^{p,q} &= \mathbf{w}_h(x_i(\xi_p), y_j(\xi_q)), \quad \mathbf{f}_d^{p,q} = \mathbf{f}_d(\mathbf{w}^{p,q}), \quad p, q = 0, 1, \dots, k \text{ and } d = 1, 2 \\ [\hat{\mathbf{f}}_1^{0,q}, \hat{\mathbf{f}}_1^{1,q}, \dots, \hat{\mathbf{f}}_1^{k,q}] &= [\hat{\mathbf{f}}_{1,i-1/2,q}, 0, \dots, 0, \hat{\mathbf{f}}_{1,i+1/2,q}], \\ [\hat{\mathbf{f}}_2^{p,0}, \hat{\mathbf{f}}_2^{p,1}, \dots, \hat{\mathbf{f}}_2^{p,k}] &= [\hat{\mathbf{f}}_{2,p,j-1/2}, 0, \dots, 0, \hat{\mathbf{f}}_{2,p,j+1/2}], \\ \hat{\mathbf{f}}_{1,i+1/2,q} &= \hat{\mathbf{f}}_1 \left( \mathbf{w}_h(x_{i+1/2}^-, y_j(\xi_q)), \mathbf{w}_h(x_{i+1/2}^+, y_j(\xi_q)) \right), \\ \hat{\mathbf{f}}_{2,p,j+1/2} &= \hat{\mathbf{f}}_2 \left( \mathbf{w}_h(x_i(\xi_p), y_{j+1/2}^-), \mathbf{w}_h(x_i(\xi_p), y_{j+1/2}^+) \right). \end{aligned}$$